Journal of the European Ceramic Society 19 (1999) 2455–2463

PII: S0955-2219(99)00107-7
0955-2219/99/$ - see front matter

Microstructure and Mechanical Properties of Al-assisted Sintered Fe/Al_2O_3 Cermets

S. Schicker,[a] T. Erny,[b] D. E. García,[a] R. Janssen[a] and N. Claussen[a]*

[a]Advanced Ceramics Group, TUHH, Technische Universität Hamburg-Harburg, 21071 Hamburg, Germany
[b]Corporate Technology, Siemens AG, 81730 München, Germany

Abstract

Fe/Al_2O_3 composites with metal contents between 23 and 35 vol% have been fabricated via Al-assisted pressureless reaction sintering. The effect of variation of oxygen partial pressure during sintering on phase development, microstructure and mechanical properties has been investigated. The formation of the spinel phase $FeO{\cdot}Al_2O_3$ is found to occur at elevated temperatures if the oxygen partial pressure during sintering exceeds a critical value. Microstructural observations and image analysis reveal that the composites exhibit a microstructure with the ceramic and the metal phase forming interpenetrating networks. The fracture toughness increases with increasing metal content and strongly depends on the phase content of the sintered specimens. In composites containing a small amount of $FeO{\cdot}Al_2O_3$, the maximum toughness is 7·1 $MPa\sqrt{m}$. A significant toughness enhancement up to 10·2 $MPa\sqrt{m}$ was achieved by avoiding the spinel formation to obtain composites consisting only of Fe and Al_2O_3. © *1999 Elsevier Science Ltd. All rights reserved.*

Keywords: Fe, sintering, composites, toughness, Al_2O_3.

1 Introduction

Compared to single phase ceramic materials, metal-reinforced ceramics exhibit attractive mechanical properties, especially improved fracture toughness. The most important mechanism responsible for the increased fracture toughness of metal-ceramic composites is crack-bridging by the ductile metal inclusions which causes crack-closure forces that shield the crack-tip.[1,2] The bridging particles are stretched to failure and energy dissipation due to plastic deformation of the ductile metal phase is the major contribution to the toughness enhancement of the composite.[3,4] As reported in the literature, [5,6] toughness enhancement increases with increasing yield strength, volume fraction and diameter of the metallic inclusions. However, there are certain conditions which must be satisfied before plastic deformation of the reinforcement phase can occur and, therefore, the toughening potential of the embedded metal phase can be fully exploited. The nature of the metal/ceramic interface strongly influences the effective use of the inherent toughness of the metal reinforcement phase. The strength of the interfacial bond between ceramic matrix and metal inclusions has to be higher than the yield strength of the metal, otherwise the crack circumvents the particles. To prevent interfacial cracking induced by stresses due to thermal mismatch between metal and ceramic, the metal inclusions should be kept under a critical size. However, partial debonding at the metal/ceramic interface has been shown to increase the extent of plastic work and, therefore, may further enhance the toughness. [6]

Al-assisted sintering of powder mixtures consisting of Fe, Al and Al_2O_3 has been recently shown to be an alternative route for low-cost fabrication of highly dense Fe/Al_2O_3-cermets.[7,8] The reduction of native oxide layers on the surface of the Fe particles by Al according to

$$Fe_2O_3 + 2{\cdot}Al \rightarrow 2{\cdot}Fe + Al_2O_3 \qquad (1)$$

$$\Delta G^0 = -840{\cdot}0 \text{ kJ/mol}$$

$$\Delta H^0 = -851{\cdot}4 \text{ kJ/mol}$$

leads to the formation of oxide-free metal/ceramic interfaces and allows the pressureless sintering of the composites to densities up to 99% theoretical density (T.D.) The Al-content of the starting mixture is consumed during the reaction sintering process to form Al_2O_3. Major phases of the resulting composites are Fe and Al_2O_3.

The present work concerns the microstructure and the mechanical properties of 23, 29 and

*To whom correspondence should be addressed Fax: + 49-40-7718-2647.

35 vol% Fe-particle-toughened Al_2O_3 composites. The influence of oxygen partial pressure on phase development, interfacial chemistry and subsequent performance of the composites has been studied.

2 Experimental Procedure

Three precursor powder mixtures, given in Table 1, were attrition milled for 7 h at 700 rpm. The 500-ml Al_2O_3-lined attrition mill (Model PE 075 Netzsch-Feinmahltechnik, Selb, FRG) was fitted with 3Y-TZP (Tosoh Co., Tokyo, Japan) stirrer arms and filled with 5 vol% of powder, 40 vol% of acetone and 50 vol% of 3-mm-diameter 3Y-TZP balls (Tosoh Co., Tokyo, Japan). After milling, the powders were dried and passed through a 200 μm sieve. Green samples with dimensions of $4 \times 5 \times 40$ mm were made by uniaxial pressing at 50 MPa, followed by cold isostatical pressing at 900 MPa. Reaction sintering was performed in vacuum (10^{-3} bar) and Ar using a heating rate of 10 K/min with a 1 h hold at 1500°C. Phase identification after thermal treatment was performed by X-ray diffractometry (XRD) using a diffractometer Type PW 1710, Philips, Eindhoven, Netherlands. The microstructure of the specimens was observed by optical microscopy (Polyvar 2, Reichert-Jung, Leica, Wetzlar, FRG), scanning electron microscopy SEM (Model JSM 840, Jeol, Tokyo, Japan) and transmission electron microscopy TEM (Model FX-2000, Jeol, Tokyo, Japan). Image analysis was done using Analysis V. 2·1 software (Soft-Imaging Software GmbH, Münster, FRG). Densities were measured with a helium pycnometer (AccuPyc 1330, Micromeritics Inc., Norcross, USA). Four-point-bending strength (span 24 and 12 mm) of the sintered specimens ($3 \times 4 \times 35$ mm) was evaluated with a universal testing machine (Type 1478, Zwick, Ulm, FRG). Samples were ground and polished with 3 μm finish on the tensile surface. Fracture toughness was determined using the ISB method.[9] Samples were indented with a Vickers diamond pyramid (Type 3212, Zwick, Ulm, FRG) at 100 N with a loading time of 10 s.

Table 1. Starting powder compositions

Designation	*Sintering atmosphere*	*Starting composition, wt%*		
		Al[a]	*Fe*[b]	*Al_2O_3*[c]
$C1_{vac}$	Vacuum	4·1	38·6	57·3
$C1_{Ar}$	Ar			
$C2_{vac}$	Vacuum	5·3	50·0	44·7
$C2_{Ar}$	Ar			
$C3_{vac}$	Vacuum	6·6	60·4	33·0
$C3_{Ar}$	Ar			

[a]Globular, Alcan 105, 5–50 μm, Alcan Int. Canada.
[b]Carbonyl iron, BASF CS, 4–5 μm, BASF FRG.
[c]Ceralox, MPA 4, 0,5 μm, Condea Chemie GmbH Brunsbüttel, FRG.

3 Results and Discussion

3.1 Influence of oxygen partial pressure on phase development

Similar to the Ni/Al_2O_3 system,[10–13] oxygen partial pressure during reaction sintering of Fe/Al_2O_3 cermets significantly influences the phase development of the composites at elevated temperatures. Figure 1(a) shows XRD results of specimens C 1_{vac} heat treated at 800, 1000 and 1500°C in vacuum. At 800°C, phase analysis only reveals Fe and Al_2O_3. A small amount of t-ZrO_2 is also present due to wear debris from 3Y-TZP milling balls. At 1000°C, peaks related to the spinel phase $FeO{\cdot}Al_2O_3$ (hercynite) appear. This spinel remains stable even after heat treatment at 1500°C. In contrast, XRD analysis of a specimen C 1_{Ar} sintered in Ar at 1500°C, does not reveal peaks corresponding to $FeO(Al_2O_3$ [Fig. 1(b)].

The iron aluminate spinel can be formed either via reaction of FeO with Al_2O_3[14] according to

$$FeO + Al_2O_3 \rightarrow FeO{\cdot}Al_2O_3 \qquad (2)$$

or via reaction between Fe and Al_2O_3, according to

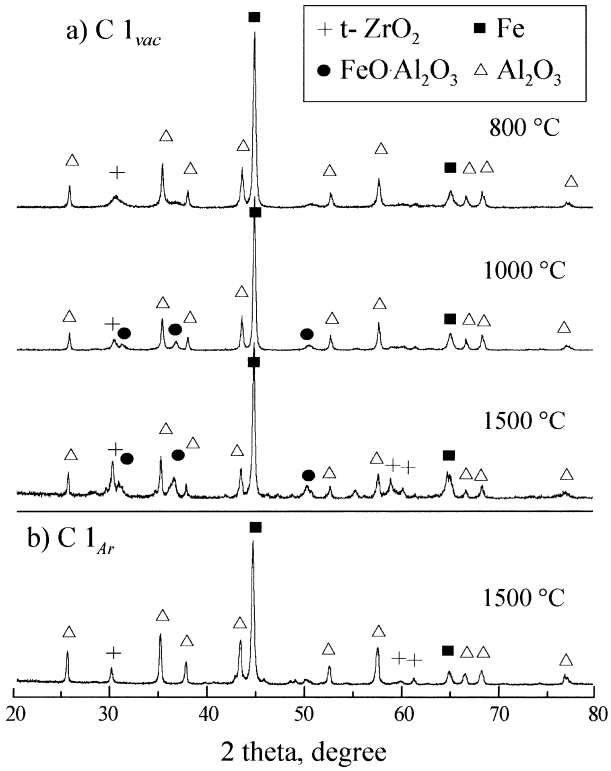

Fig. 1. XRD diagrams of (a) $C1_{vac}$ samples heat treated at 800, 1000 and 1500°C and (b) $C1_{Ar}$ sintered at 1500°C.

$$\mathrm{Fe(s)} + 0{\cdot}5{\cdot}\mathrm{O_2(g)} + (1+x){\cdot}\mathrm{Al_2O_3(s)} \leftrightarrow \mathrm{FeO{\cdot}(1+x)Al_2O_3(s)} \quad (3)$$

if p_{o_2} exceeds a temperature dependent critical value.[15,16]

Due to the absence of FeO in the critical temperature range between 1000 and 1500°C, it can be assumed that hercynite formation in Fe/Al_2O_3 cermets occurs via the reaction expressed in eqn (3). Oxygen partial pressure in the Fe + FeO·(1 + *x*)-Al_2O_3/Fe + Al_2O_3 equilibrium has been experimentally measured by Elfrefaie and Schmeltzer[16] in the temperature range between 800 and 1300°C and is given by

$$\log p_{\mathrm{o_2}} = -\frac{30500}{T} + 7{\cdot}154 \quad (4)$$

with an error limit log $p_{\mathrm{o_2}} = \pm 0{\cdot}1$ atm. Equation (4) is plotted in Fig. 2. The values for $p_{\mathrm{o_2}}$ calculated following eqn (4) stand in good agreement with the experimental data published by Petrick *et al.*[15] ($p_{\mathrm{o_2}}(1300°\mathrm{C}) = 5{\cdot}7111\times10^{-8}$ Pa). In the temperature range between 1300 and 1500°C the curve has been extrapolated. Figure 2 shows that the critical $p_{\mathrm{o_2}}$ for spinel formation increases with increasing temperature from 5×10^{-17} Pa at 800°C to approximately 10^{-5} Pa at 1500°C. XRD analysis reveals that control during reaction sintering allows to influence the phase development of Fe/Al_2O_3 cermets. During sintering in vacuum, $p_{\mathrm{o_2}}$ exceeds the critical value of 10^{-5} Pa and, therefore, spinel formation is inevitable. In contrast, the low $p_{\mathrm{o_2}}$ of the Ar-atmosphere allows one to obtain only Fe and Al_2O_3.

In Al-assisted sintered Fe/Al_2O_3 cermets, spinel formation takes place only at temperatures above 1000°C. This can be attributed to the increasing diffussivity at elevated temperatures or to the presence of Al in the starting mixtures of the reaction sintered composites. Small amounts of residual Al,

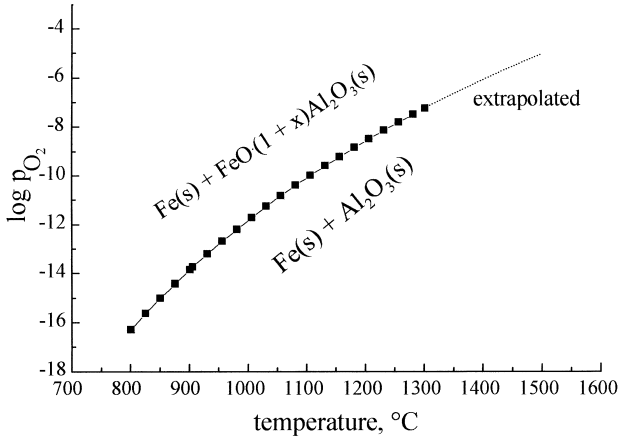

Fig. 2. Critical oxygen partial pressure for Fe-Al_2O_3/Fe-FeO·Al_2O_3 equilibrium as a function of temperature.

which is not consumed by the reduction of Fe oxides on the surfaces of Fe particles at temperatures ~600°C[8] can form a solid solution with Fe. The reaction of a Fe(Al)-solid solution with atmospheric oxygen can be written as[16]

$$2{\cdot}\mathrm{Al_{(solid\,solution)}} + 1{\cdot}5{\cdot}\mathrm{O_2} \rightarrow \mathrm{Al_2O_3} \quad (5)$$

$$\Delta G^\circ = -1582{\cdot}3 \text{ kJ/mol}$$

$$\Delta H^\circ = -1675{\cdot}7 \text{ kJ/mol}$$

Due to the high oxygen affinity of Al, this reaction prevents FeO·Al_2O_3 formation and, therefore, may be responsible for the delay in spinel formation until after the whole amount of Al present in the starting mixture is consumed to form Al_2O_3 according to eqns (1) and (5), respectively.

3.2 Microstructure

The typical microstructures of Al-assisted sintered Fe/Al_2O_3 cermets are displayed in Fig. 3(a)–(c) showing the change in the morphology of the metal phase with increasing metal content of the composites. At low metal contents, nearly spherical metal particles are embedded within the ceramic matrix while, at higher metal contents, flake-shaped metal ligaments form an interconnected network. To exactly determine the size of the metal inclusions as well as the metal phase content after reaction sintering and the penetration of the metal phase, a quantitative characterization of the microstructure using image analysis was performed. After Poech and Ruhr[17] the three-dimensional penetration of one phase in a composite material can be described by the degree of skeleton formation in a two-dimensional cut. Figure 4 shows an example for the reduction of the ceramic and the metal ligaments to skeleton lines in the microstructure of composite $C3_{vac}$ and the determination of the respective skeleton line lengths. The three-dimensional penetration of the metal phase Ψ_m can be calculated from eqn (6)

$$\Psi_m = \frac{S_m}{S_m + S_c} \quad (6)$$

where S_m and S_c are the skeleton line length of the metal and the ceramic phase, respectively.

Image analysis results of the sintered specimens are listed in Table 2. As a result of Al oxidation during milling[18] and reaction sintering, the metal content of the sintered specimens is significantly lower than the metal content of the starting mixtures; it is 23 vol% for $C1_{vac}$, 29 vol% for $C2_{vac}$ and 35 vol% for $C3_{vac}$, respectively. The skeleton line length determination reveals at that at metal

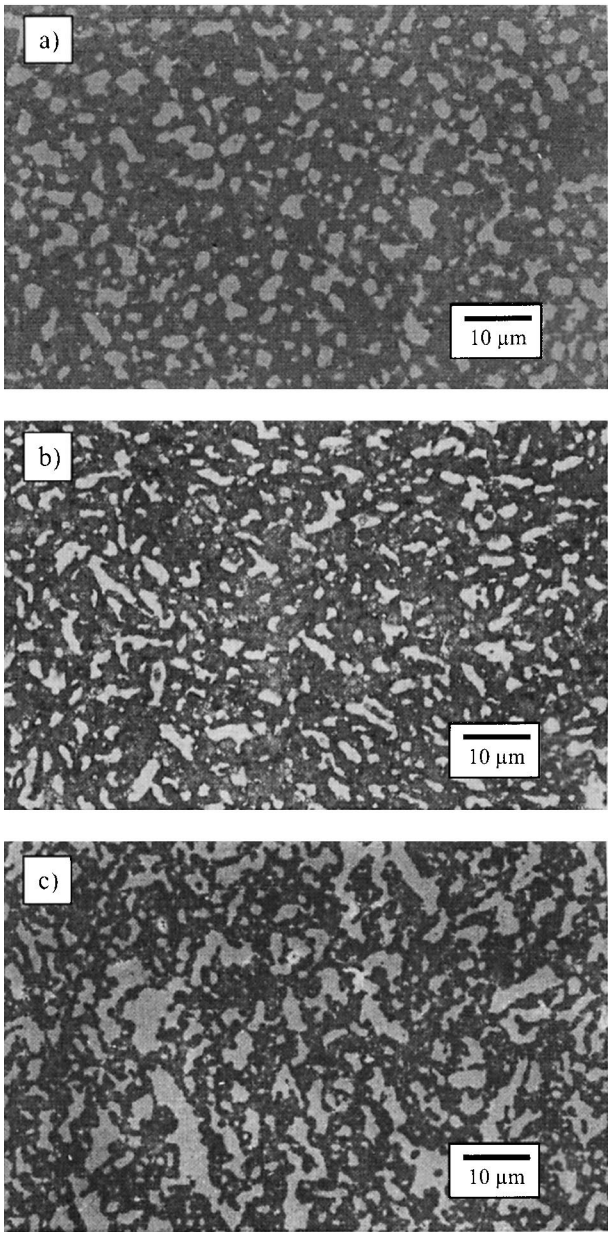

Fig. 3. Typical microstructures of Al-assisted sintered Fe/Al_2O_3-cermets (a) $C1_{vac}$, (b) $C2_{vac}$, (c) $C3_{vac}$.

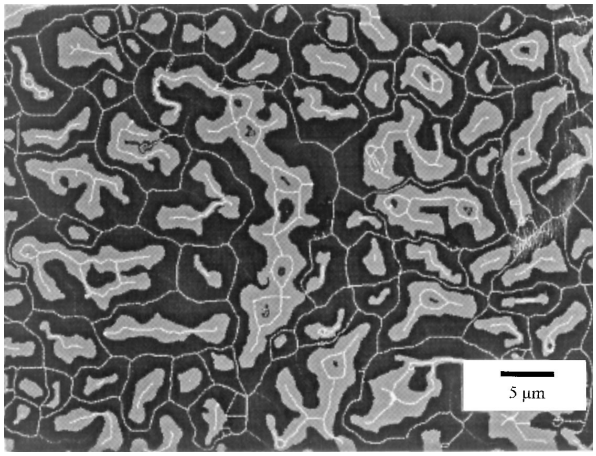

Fig. 4. Skeleton line length determination in a binary image showing the microstructure of composite $C3_{vac}$.

contents ~30 vol% the metal and the ceramic phase in Al-assisted sintered Fe/Al_2O_3 cermets form interpenetrating networks, which is similar to that achieved by infiltration of porous Al_2O_3 preforms[4,19,20] or by reaction forming, e.g. directed metal oxidation (DIMOX)[21] or reactive metal penitration (RMP).[22] The increase of the metal content from 23 to 29 vol% is accompanied by a significant increase of the penetration implying that the medium ligament diameter of the metal phase remains nearly constant. This correlation is confirmed by the experimentally determined values of 1·5 μm for composite $C1_{vac}$ and 1·7 μm for composite $C2_{vac}$. Only further increase of the metal content up to 35 vol% Fe leads to formation of metal inclusions with a medium diameter of 2·3 μm.

A significant influence of the sintering atmosphere on microstructural development especially, on the metal inclusion size, was not found. Optical microscopy and SEM did not reveal any information about the morphology of the spinel phase indicating very small grain sizes or that the spinel is located at the metal/ceramic interface. The formation of FeO·Al_2O_3 consumes Fe and, therefore, inevitably leads to a decrease of the content of ductile metal phase in the composite. However, taking into consideration the error limits of the image analysis (± 1 vol%) the decrease of the metal content caused by hercynite formation is too small to be recorded by image analysis.

3.3 Mechanical properties

The mechanical properties of the reaction sintered Fe/Al_2O_3 cermets are displayed in Fig. 5. Bending strength and fracture toughness of the composites sintered in vacuum and Ar are given as a function of metal content. With increasing metal content, the bending strength of composites sintered in vacuum decreases from 641 MPa (composition $C1_{vac}$) to 503 MPa (composition $C3_{vac}$). This can be correlated with the final densities of the sintered specimens, which were 99% T.D. in the 23 vol% Fe composite, 95% T.D. in the 29 vol.% Fe composite and 94% T.D. in the 35 vol% Fe composite, respectively. A significant influence of the sintering atmosphere on sintering behavior, final densities and bending strength cannot be observed. As expected, the fracture toughness of the composites increases with increasing metal content. In composites sintered in vacuum, K_{IC} increases from 4·7 MPa$\sqrt{m}$ in composition $C1_{vac}$ to 7·1 MPa $\sqrt{m}$ in composition $C3_{vac}$. Sintering in Ar results in a 30–50% enhanced fracture toughness. K_{IC} of the composites is determined to be 6·1 MPa $\sqrt{m}$ ($C1_{Ar}$), 7·8 MPa $\sqrt{m}$ ($C2_{Ar}$) and 10·2 MPa $\sqrt{m}$ ($C3_{Ar}$), respectively.

Crack path observations were performed to investigate the mechanisms responsible for enhanced fracture toughness of the composites compared to single phase Al_2O_3. Figure 6 shows the interaction of a crack caused by indentation with iron particles in a composites $C3_{vac}$. The crack is either bridged or deflected by the metal inclusions. Figure 7 shows the fracture surface of composite $C3_{vac}$. Stretched iron particles, still attached to the Al_2O_3-matrix can be observed. Cavities resulting from the pull out of iron particles due to a weak metal/ceramic interface can only be found very rarely. The fracture surface of specimen $C2_{vac}$ (Fig. 8) shows that even in composites with lower metal contents fracture is mainly transgranular, again indicating a strong interfacial bond between Al_2O_3 and Fe. Fig. 9 shows the detail magnification of an Fe ligament stretched to failure in the fracture surface of composite $C3_{vac}$. Partial debonding at the interface is clearly visible, resulting in a larger crack opening displacement upon ductile phase rupture and therefore having a beneficial effect on fracture toughness enhancement.

Following Ashby *et al.*[6] the toughness enhancement in metal-reinforced composite materials, ΔK_{IC}, contributed by crack bridging of ductile metal inclusions is proportional to the square root of the product of the volume fraction, v_{me}, and the particle radius, r, of the inclusions,

Table 2. Results of the image analysis

Composition	*Metal content of the starting mixture, vol%*	*Metal content after reaction sintering, vol%*	*Largest metal phase diameter, μm*	*Medium metal phase diameter, μm*	*Degree of three-dimensional penetration of the metal phase*
$C1_{vac}$	31	23	10·6	1·5	0·06
$C2_{vac}$	43	29	13·3	1·7	0·21
$C3_{vac}$	55	35	19·9	2·3	0·34

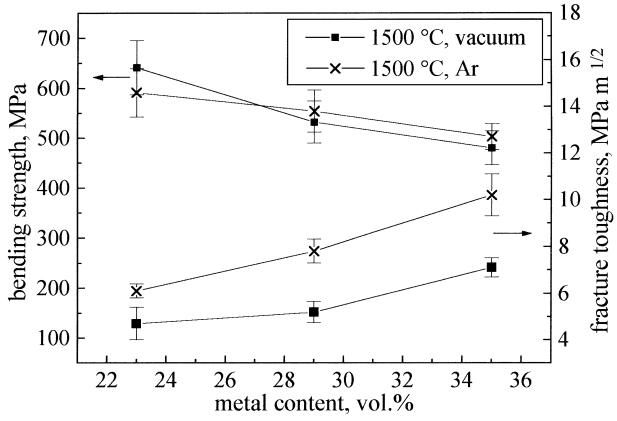

Fig. 5. Mechanical properties of Fe-reinforced Al_2O_3 composites after sintering in vacuum and Ar as a function of metal content.

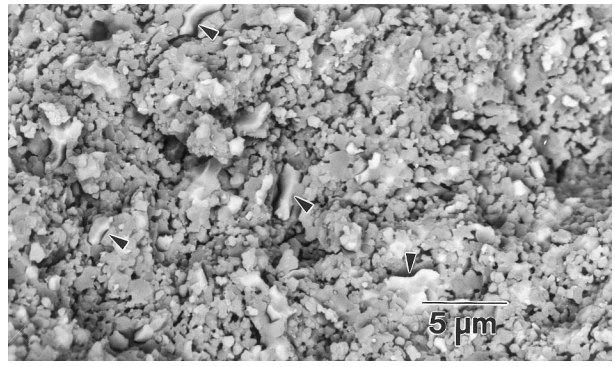

Fig. 7. SEM micrograph of fracture surface of specimen $C3_{vac}$.

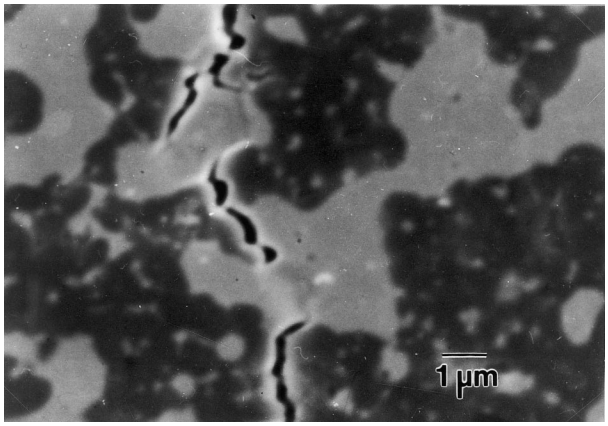

Fig. 6. Interaction of indentation crack with Fe-ligaments in sample $C3_{vac}$.

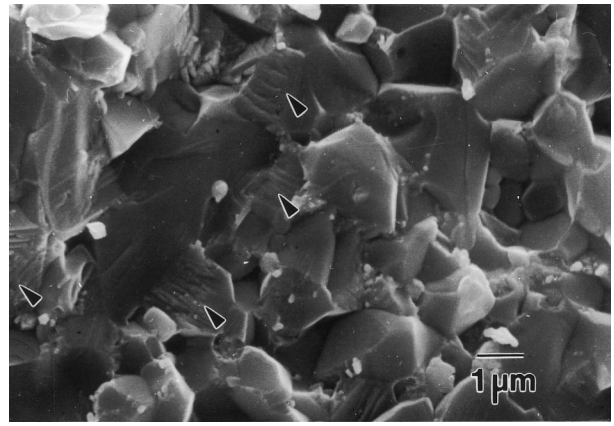

Fig. 8. SEM micrograph of fracture surface of composite $C1_{vac}$, showing transgranular crack propagation.

$$K_{IC} = \sqrt{a_{me} \cdot \chi \cdot E \cdot \sigma_0 \cdot r \cdot v_{me}} \quad (7)$$

where a_{me} is the area fraction of the metal reinforcement phase intercepted by the crack, χ is a dimensionless constant, σ_0 is the yield strength and E the Young's modulus of the reinforcement phase. In Fig. 10, ΔK_{IC}, calculated from the experimental results shown in Fig. 5, is plotted against $\sqrt{r \cdot v_{me}}$ and a linear relationship is found for both composites sintered in vacuum and in Ar which indicates, in good accordance with the SEM observations, that in both cases crack deflection around metal inclusions is limited and plastic deformation and crack bridging is the major toughening mechanism.

However, SEM observations reveal that, in composites consisting only of Fe and Al_2O_3 ($C1_{Ar}$, $C2_{Ar}$, $C3_{Ar}$) as well as in specimens containing a small amount of hercynite ($C1_{vac}$, $C2_{vac}$, $C3_{vac}$), only a limited fraction between ~25 and ~50% of the metal phase present in the fracture surface show plastic deformation (Fig. 7). It can qualitatively be estimated that the fraction of metal particles participating in plastic deformation and crack bridging increases with increasing metal content, which can be attributed to the change in the morphology of the metal phase from isolated small particles to flake-shaped interconnected ligaments and is slightly higher in the cermets containing only Fe and Al_2O_3 ($C1_{Ar}$, $C2_{Ar}$, $C3_{Ar}$).

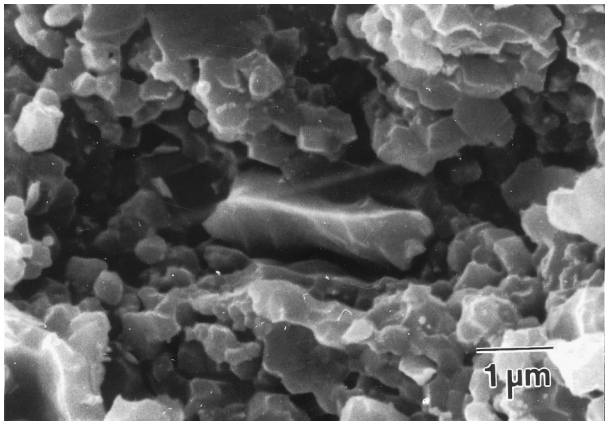

Fig. 9. Fe ligament stretched to failure in fracture surface of composite $C3_{vac}$, partial debonding at the metal/ceramic interface is clearly visible.

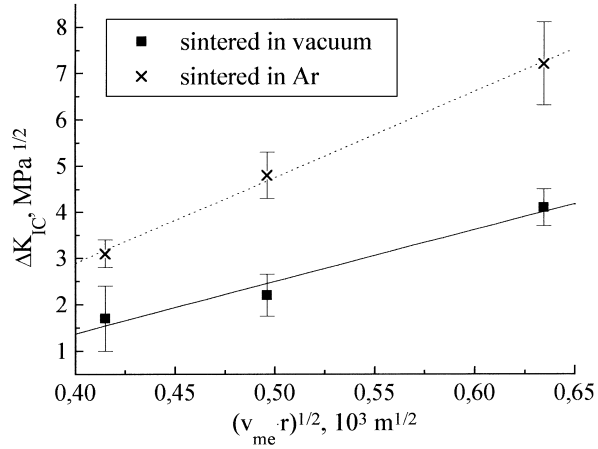

Fig. 10. ΔK_{IC} of Fe/Al_2O_3 cermets as a function of the square root of the product of metal volume fraction and inclusion size [eqn. (7)].

The influence of interface chemistry and interfacial bonding on mechanical performance of metal reinforced ceramics has been extensively discussed in the literature.[10,11,24] To determine the morphology of hercynite and whether it forms an intermediate phase at the Fe/Al_2O_3 interface, similar to $NiO{\cdot}Al_2O_3$ which was found to form an interlayer between Ni and Al_2O_3,[12,13] TEM studies have been performed. Figure 11 shows a TEM bright field image of the microstructure of a specimen $C1_{vac}$ after sintering at 1500°C. Fe Particles 1–3 μm are embedded within the Al_2O_3 matrix which has grain sizes between 0·5 and 3 μm. Small Fe grains decorating the Al_2O_3 grain boundaries are typical for the microstructure of Al-assisted sintered cermets as well as small (50–300 nm) Al_2O_3 grains located at the grain boundaries of metal inclusions. Within the Fe and Al_2O_3 grains, dislocations due to the thermal mismatch between the ceramic and metal phase can be observed. Despite these stress-induced defects, the dark field image in Fig. 12 shows that Fe particles consist mainly of domains of one crystallographic orientation. Most inclusions $< 1\,\mu$m were found to be single crystalline. The metal/ceramic interface is shown in Fig. 13 at higher magnification, giving no indication of an intermediate phase between Fe and Al_2O_3. However, due to the resolution limit of the micrograph, the presence of a thin interlayer < 2–3 nm can not be excluded. The bright field TEM micrograph of a composite $C1_{vac}$ (Fig. 14) reveals that the major amount of the spinel phase exhibits a granular

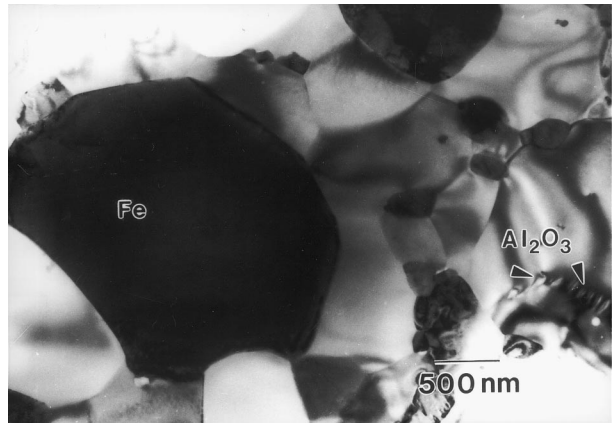

Fig. 11. TEM bright field image of specimen $C1_{vac}$, showing the formation of dislocations due to thermal stresses.

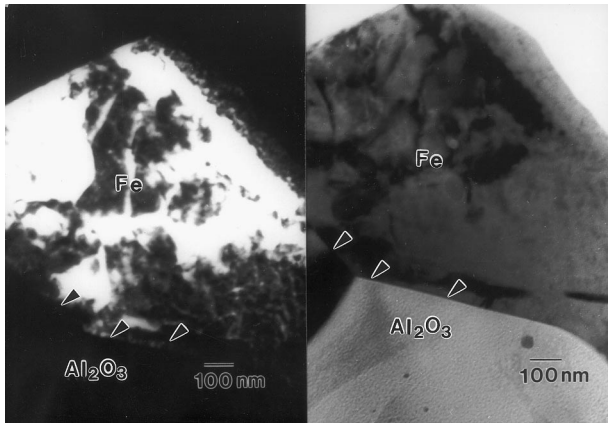

Fig. 12. TEM bright and dark field images of an Fe inclusion, showing that the metal particles mainly consist of domains of one crystallographic orientation.

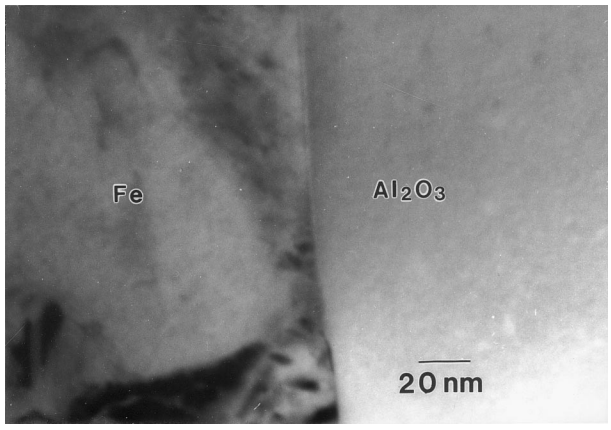

Fig. 13. TEM micrograph of Fe/Al_2O_3 interface in composite $C1_{vac}$.

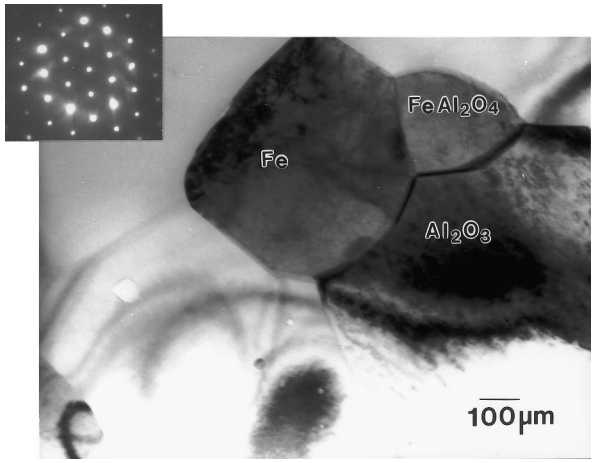

Fig. 14. TEM image of specimen $C1_{vac}$ sintered in vacuum, showing that the spinel phase exhibits granular morphology.

morphology. FeO·Al_2O_3 can be identified by Small Angle Diffraction, the diffraction pattern shows a $\bar{1}11$ orientation of the fcc lattice. The spinel grains with typical sizes between 200 and 300 nm are usually located between Fe and Al_2O_3 grains.

Fracture surface and microstructural features imply that the composites $C1_{vac}$, $C2_{vac}$ and $C3_{vac}$ lose ductility due to the FeO·Al_2O_3 formation when compared to the spinel-free samples $C1_{Ar}$, $C2_{Ar}$ and $C3_{Ar}$. Thus, it has to be assumed that, beside spinel grains, a very thin spinel layer (a few atoms thick), which can only be detected by extensive HRTEM studies, is formed at the Fe/Al_2O_3 interface reducing the interfacial bonding. Thermodynamic analysis of spinel formation at Fe/Al_2O_3 interfaces has been published by Trumble[25] but the authors are aware of no experimental work on chemical reactions at solid Fe/Al_2O_3 interfaces.

In the Ni/Al_2O_3 system, spinel-interphase formation and its influence on the strength of the metal/ceramic interface has been extensively discussed in the literature. Some authors claim that a thin NiO·Al_2O_3-layer at the interface between Ni and Al_2O_3 has a beneficial effect on interfacial bonding,[26,27] while other studies report on the detrimental effect of spinel formation on the strength of the metal/ceramic interface.[11]

Mechanical testing results in the present paper indicate that FeO·Al_2O_3 weakens the Fe/Al_2O_3 interface. The weakness of the spinel/Fe interface may be due to residual thermal stresses resulting from the thermal expansion mismatch or the interface may be intrinsically weak. According to Kohle *et al.*,[28] the residual stresses σ_{th} at the metal/ceramic interface due to the difference in coefficient of thermal expansion (CTE) can be calculated from

$$\sigma_{th} = \frac{\left[(1+\nu_c)^2\cdot\alpha_c - (1+\nu_{me})^2\cdot\alpha_{me}\right]\cdot\Delta T_s}{\frac{(1-2\cdot\nu_{me})\cdot(1+\nu_{me})}{E_{me}} + \frac{(1+\nu_c)}{E_c}} \quad (8)$$

where ν_c and ν_{me} are the Poisson ratios of the ceramic and the metal phase, E_c and E_{me} are the Young's moduli of the ceramic and the metal phase and ΔT_S is the temperature difference between sintering temperature and room temperature. From eqn (8), the stresses at the Fe/Al_2O_3 interface are 1·97 GPa, at the Fe/FeO·Al_2O_3 interface 2·2 GPa, being almost alike due to the similar CTE's of FeO·Al_2O_3 and Al_2O_3. Thus, an Fe/spinel interface may be considered to be intrinsically weak. Several authors report on the high strength of clean Fe/Al_2O_3 interfaces.[29,30]

Nevertheless, even in composites $C1_{Ar}$, $C2_{Ar}$ and $C3_{Ar}$, without spinel, thermal stresses in the range of 2 GPa may cause interfacial debonding or microcracking. According to eqn. (7), ΔK_{IC} increases with increasing size of the reinforcing particles. However, large metal inclusions were found to cause thermally induced interfacial cracking. The critical size of metal inclusions for interfacial cracking, D_c, can be calculated from[31,32]

$$D_c = \frac{8 \cdot K_{IC,c}^2}{\sigma_{th}^2 \cdot \left[(1+\nu_c) + 2 \cdot \frac{E_c}{E_{me}} \cdot (1 - 2 \cdot \nu_{me}) \right]} \quad (9)$$

where $K_{IC,c}$ is the fracture toughness of the ceramic matrix. For Fe inclusions embedded in an Al_2O_3 matrix, D_c is 5·98 μm indicating that most of the metal ligaments in Al-assisted sintered Fe/Al_2O_3 cermets are smaller than D_c.

4 Conclusions

1. Formation of the spinel phase $FeO{\cdot}Al_2O_3$ (hercynite) was found to occur at elevated temperatures if the oxygen partial pressure during sintering exceeds a temperature-dependent critical value, of$\sim 10^{-5}$ Pa at 1500°C.
2. Spinel formation can be avoided by sintering in Ar.
3. The composites exhibit fine grained microstructures with the ceramic and the metal phase forming interpenetrating networks. The size of the metal inclusions is between 1·5 and 2·3 μm.
4. The metal particle size was found to be smaller than the critical value at which interfacial cracking due to thermal stresses induced by the mismatch of CTE's of the metal and the ceramic phase occurs.
5. Four point bending strengths decrease with increasing metal content due to residual porosity of the sintered specimens and varies between 503 and 641 MPa.
6. Fracture toughness increases with increasing metal content and strongly depends on the phase content of the sintered specimens. In composites containing a small amount of $FeO{\cdot}Al_2O_3$ the maximum toughness values were determined to be 7·1 MPa$\sqrt{m}$. A significant enhancement of the toughness up to 10·2 MPa$\sqrt{m}$ was achieved by avoiding the spinel formation to obtain composites consisting only of Fe and Al_2O_3.
7. Plastic deformation and crack-bridging was found to be the major toughening mechanism in Al-assisted sintered Fe/Al_2O_3-cermets.
8. Fracture surface and crack path observations indicate a strong metal/ceramic interfacial bonding, preventing a pull-out of the metal particles. However, in some cases partial debonding at the interface, which benefits the toughness enhancement, can be observed.
9. TEM observations reveal that the spinel phase exhibits a granular morphology. However, it can be assumed that a thin $FeO{\cdot}Al_2O_3$ interlayer at the Fe/Al_2O_3 interface is also present weakening the metal/ceramic bond and therefore declining the fracture toughness of the composites.
10. Thermal stresses due to the mismatch of CTE's were found not to be responsible for the weakness of a Fe/spinel interface. Hence, compared to the strength of a clean Fe/Al_2O_3 interface, the Fe/$FeO{\cdot}Al_2O_3$ interface seems to be intrinsically weak.

Acknowledgements

The authors wish to thank BMBF for financial support under contract No 03N3026 and Axel Krupp for technical assistance.

References

1. Krstic, J. T., On the fracture of brittle-matrix/ductile-particle composites. *Philos. Mag., A*, 1983, **48**(5), 695–708.
2. Flinn, B. D., Rühle, M. and Evans, A. G., Toughening in Composites of Al_2O_3 Reinforced with Al. *Acta Metall.*, 1989, **37**(11), 3001–3006.
3. Rödel, J., Sindel, M., Dransmann, M., Steinbrech, R. W. and Claussen, N., R-Curve behaviour in ceramic composites produced by directed metal oxidation. *J. Eur. Ceram. Soc.*, 1994, **14**, 153–161.
4. Claussen, N., Knechtel, M., Prielipp, H. and Rödel, J., Metcers — a strong variant of cermets. *cfi/Ber. DKG*, 1994, **71**(6), 301–303.
5. Sigl, L. S., Mataga, P. A., Dalgleish, B. J., McMeeking, R. M. and Evans, A. G., On the toughness of brittle materials reinforced with a ductile phase. *Acta Metall.*, 1988, **36**(4), 945–953.
6. Ashby, M. F., Blunt, F. J. and Bannister, M., Flow characteristics of highly constrained metal wires. *Acta Metall.*, 1989, **37**(7), 1847–1857.
7. Schicker, S., García, D. E., Janssen, R. and Claussen, N. German Patent Application DE 19619500, filing date 14.5.1996.
8. Schicker, S., García, D. E., Bruhn, J., Janssen, R. and Claussen, N., Reaction processing of Al_2O_3 composites containing iron and iron aluminides. *J. Am. Ceram. Soc.*, 1997, **80**(9), 2294–2300.
9. Chantikul, P., Anstis, G. R., Lawn, B. R. and Marshall, D. B., A critical evaluation of indentation techniques for measuring fracture toughness: II, Strength method. *J. Am. Ceram. Soc.*, 1981, **64**(9), 539–540.
10. Sun, X. and Yeomans, J., Microstructure and fracture toughness of nickel particle toughened alumina matrix composites. *J. Mater. Sci.*, 1996, **31**, 875–880.
11. Sun, X. and Yeomans, J., Optimization of a ductile-particle-toughened ceramic. *J. Am. Ceram. Soc.*, 1996, **79**(10), 2701–2717.
12. Trumble, K. P. and Rühle, M., The role of oxygen for the spinel interphase formation at diffusion-bonded Ni/Al_2O_3 interfaces. *Z. Metallkd.*, 1990, **81**(10), 749–755.
13. Trumble, K. P. and Rühle, M., The thermodynamics of spinel interphase formation at diffusion-bonded Ni/Al_2O_3 interfaces. *Acta Metall. Mater.*, 1991, **39**(8), 1915–1924.
14. Prescott, R. and Graham, M. J., The oxidation of iron-aluminum alloys. *Oxidation of Metals*, 1992, **38**(1/2), 73–87.
15. Petric, A., Jakob, K. T. and Alcock, C. B., Thermodynamic properties of Fe_3O_4-$FeAl_2O_4$ spinel solid solutions. *J. Am. Ceram. Soc.*, 1981, **64**(11), 632–639.
16. Elrefaie, F. A. and Smeltzer, W. W., Thermodynamics of the system iron-aluminum-oxygen between 1073 K and 1573 K. *Metall. Trans. B*, 1983, **14B**, 85–93.
17. Poech, M. and Ruhr, D., Die quantitative Charakterisierung der Gefügeanordnung. *Prakt. Met., Sonderbd.*, 1993, **24**, 385–391.

18. Schicker, S. García, D. E. Gorlov, I. Janssen, R. and Claussen, N. Wet milling of $Fe/Al/Al_2O_3$ and $Fe_2O_3/Al/Al_2O_3$ powder mixtures for reaction sintering of Al_2O_3-aluminides. sumitted to *J. Am. Ceram. Soc*.
19. Jangg, V. G., Kieffer, R., Gugel, E., Kollwentz, W. and Jicinsky, G., Applications of the infiltration technique to the manufacture of cermets. *Ber. Dt. Keram. Ges*., 1971, **48**, 262–268.
20. Wu, S., Gesing, A. J., Travitzky, N. A. and Claussen, N., Fabrication and properties of Al-infiltrated RBAO-based composites. *J. Eur. Ceram. Soc*., 1991, **7**, 277–281.
21. Newkirk, M. S., Urquhart, A. W., Zwicker, H. R. and Breval, E., Formation of Lanxide™ ceramic composite materials. *J. Mater. Res*., 1986, **1**, 81–89.
22. Loehman, R. E., Ewsuk, K. and Tomsia, A. P., Synthesis of Al_2O_3-Al composites by reactive melt penetration. *J. Am. Ceram. Soc*., 1996, **79**(1), 27–32.
23. Zhang, X., Lu, G., Hoffmann, M. and Metselaar, R., Properties and interface structures of Ni and Ni-Ti alloy toughened Al_2O_3 ceramic composites. *J. Eur. Ceram. Soc*., 1995, **15**, 225–232.
24. Lourdin, P., Juvé, D. and Tréheux, D., Nickel-alumina bonds: mechanical properties related to interfacial chemistry. *J. Eur. Ceram. Soc*., 1996, **16**, 745–752.
25. Trumble, K. P., Thermodynamic analysis of aluminate formation at Fe/Al_2O_3 and Cu/Al_2O_3 interfaces. *Acta Metall. Mater*., 1992, **40** (Suppl.), S105.
26. Pepper, S. V., Shear strength of metal-sapphire contacts. *J. Appl. Phys*., 1976, **47**(3), 801–808.
27. de Bruin, H. J., Moodie, A. F. and Warble, C. E., Ceramic-metal reaction welding. *J. Mater. Sci*., 1972, **7**, 909–918.
28. Kohle, R., Hui, C. Y., Ustundag, E. and Sass, S. L., Residual thermal stresses and calculations of the critical metal particle size for interfacial crack extension in metal-ceramic matrix composites. *Acta Mater*., 1996, **44**(1), 279–287.
29. Nicholas, M., The strength of metal/alumina interfaces. *J. Mater. Sci*., 1968, **3**, 571–576.
30. Johnson, K. H. and Pepper, S. V., Molecular-orbital model for metalo-saphire interfacial strength. *J. Appl. Phys*., 1982, **53**(10), 6634–6637.
31. Davidge, R. W. and Green, T. J., The strength of two-phase ceramic/glass materials. *J. Mater. Sci*., 1968, **3**, 629–634.
32. Magley, D. J., Winholtz, R. A. and Faber, K. T., Residual stresses in a two-phase microcracking ceramic. *J. Am. Ceram. Soc*., 1990, **73**(6), 1641–1644.